

DeepJDOT: Deep Joint distribution optimal transport for unsupervised domain adaptation

Bharath Bhushan Damodaran¹, Benjamin Kellenberger², Rémi Flamary³,
Devis Tuia², Nicolas Courty¹

¹ Université de Bretagne Sud

IRISA, UMR 6074, CNRS

{bharath-bhushan.damodaran,nicolas.courty}@irisa.fr

² University of Wageningen, Netherlands

{name.surname}@wur.nl

³ Université Côte dAzur

Lagrange, UMR 7293, CNRS, OCA

remi.flamary@unice.fr

Abstract. In computer vision, one is often confronted with problems of domain shifts, which occur when one applies a classifier trained on a source dataset to target data sharing similar characteristics (e.g. same classes), but also different latent data structures (e.g. different acquisition conditions). In such a situation, the model will perform poorly on the new data, since the classifier is specialized to recognize visual cues specific to the source domain. In this work we explore a solution, named DeepJDOT, to tackle this problem: through a measure of discrepancy on joint deep representations/labels based on optimal transport, we not only learn new data representations aligned between the source and target domain, but also simultaneously preserve the discriminative information used by the classifier. We applied DeepJDOT to a series of visual recognition tasks, where it compares favorably against state-of-the-art deep domain adaptation methods.

Keywords: Deep Domain Adaptation, Optimal Transport

1 Introduction

The ability to generalize across datasets is one of the holy grails of computer vision. Designing models that can perform well on datasets sharing similar characteristics such as classes, but also presenting different underlying data structures (for instance different backgrounds, colorspace, or acquired with different devices) is key in applications where labels are scarce or expensive to obtain. However, traditional learning machines struggle in performing well out of the datasets (or *domains*) they have been trained with. This is because models generally assume that both training (or *source*) and test (or *target*) data are issued from the same generating process. In vision problems, factors such as objects position, illumination, number of channels or seasonality break this assumption

and call for adaptation strategies able to compensate for such shifts, or *domain adaptation* strategies [1].

In a first rough subdivision, domain adaptation strategies can be separated into *unsupervised* and *semi-supervised* domain adaptation: the former assumes that no labels are available in the target domain, while the latter assumes the presence of a few labeled instances in the target domain that can be used as reference points for the adaptation. In this paper, we propose a contribution for the former, more challenging case. Let $\mathbf{x}^s \in \mathbb{X}^S$ be the source domain examples with the associated labels $y^s \in \mathbb{Y}^S$. Similarly, let $\mathbf{x}^t \in \mathbb{X}^T$ be the target domain images, but with unknown labels. The goal of the unsupervised domain adaptation is to learn the classifier f in the target domain by leveraging the information from the source domain. To this end, we have access to a source domain dataset $\{\mathbf{x}_i^s, y_i^s\}_{i=1, \dots, n^s}$ and a target domain dataset $\{\mathbf{x}_i^t\}_{i=1, \dots, n^t}$ with only observations and no labels.

Early unsupervised domain adaptation research tackled the problem as the one of finding a common representation between the domains, or a latent space, where a single classifier can be used independently from the datapoint’s origin [2, 3]. In [4], the authors propose to use discrete optimal transport to match the shifted marginal distributions of the two domains under constraints of class regularity in the source. In [5] a similar logic is used, but the joint distributions are aligned directly using a coupling accounting for the marginals and the class-conditional distributions shift *jointly*. However, the method has two drawbacks, for which we propose solutions in this paper: 1) first, the JDOT method in [5] scales poorly, as it must solve a $n_1 \times n_2$ coupling, where n_1 and n_2 are the samples to be aligned; 2) secondly, the optimal transport coupling γ is computed between the input spaces (and using a ℓ_2 distance), which is a poor representation to be aligned, since we are interested in matching more semantic representations supposed to ease the work of the classifier using them to take decisions.

We solve the two problems above by a strategy based on deep learning. On the one hand, using deep learning algorithms for domain adaptation has found an increasing interest and has shown impressive results in recent computer vision literature [6–9]. On the other hand (and more importantly), a Convolutional Neural Network (CNN) offers the characteristics needed to solve our two problems: 1) by gradually adapting the optimal transport coupling along the CNN training, we obtain a scalable solution, an approximated and stochastic version of JDOT; 2) by learning the coupling in a deep layer of the CNN, we align the representation the classifier is using to take its decision, which is a more semantic representation of the classes. In summary, we learn jointly the embedding between the two domains and the classifier in a single CNN framework. We use a domain adaptation-tailored loss function based on optimal transport and therefore call our proposition *Deep Joint Distribution Optimal Transportation (DeepJDOT)*.

We test DeepJDOT on a series of visual domain adaptation tasks and compare favorably against several recent state of the art competitors.

2 Related works

Unsupervised domain adaptation. Unsupervised domain adaptation considers the situation where the source domain carries labeled instances, while the target domain is unlabeled, yet accessible during training [10]. Earlier approaches consider projections aligning the data spaces to each other [2, 11, 12], thus trying to exploit shift-invariant information to match the domains in their original (input) space. Later works extended such logic to deep learning algorithms, typically by weight sharing [6]/reconstruction [13], by adding Maximum Mean Discrepancy (MMD) and association-based losses between source and target layers [14–16]. Another major wave of development is found in the inclusion of adversarial loss functions pushing the CNN to be unable to discriminate whether a sample comes from the source or the target domain [7, 8, 17]. Finally, the most recent works extend this adversarial logic to the use of GANs [18, 19], for example using two GAN modules with shared weights [9], forcing image to image architectures to have similar activation distributions [20] or simply fooling a GAN’s discriminator discerning between domains [21]. This adversarial image generation based method [18–20] uses a class-conditioning or cycle consistency term to learn the discriminative embedding, such that the semantically similar images in both domains are projected into close vicinity in the embedding space. Our proposed DeepJDOT use the concept of a shared embedding for both domains [17] and is built on a similar logic as MMD-based methods, yet adding a clear discriminative component to the alignment: the proposed DeepJDOT associates representation and discriminative learning, since the optimal transport coupling ensures that distributions are matched, while *i)* the JDOT class loss performs source label propagation to the target samples and *ii)* the fact that the coupling is learned in deep layers of the CNN ensures discrimination power.

Optimal transport in domain adaptation. Optimal transport [22–24] has been used in domain adaptation to learn the transformation between domains [4, 25, 26], with associated theoretical guarantees [27]. In those works, the coupling γ is used to transport (i.e. transform) the source data samples through an estimated mapping called barycentric mapping. Then, a new classifier is trained on the transported source data representation. But those different methods can only address problems of small to medium sizes because they rely on the exact solution of the OT problem on all samples. Very recently, Shen *et al.* [28] used the Wasserstein distance as a loss in a deep learning setting to promote similarities between embedded representations using the dual formulation of the problem exposed in [29]. However, none of those approaches considers an adaptation w.r.t. the discriminative content of the representation, as we propose in this paper with DeepJDOT.

3 Optimal transport for domain adaptation

Our proposal is based on optimal transport. After recalling the associated basic notions and its relation with domain adaptation, we detail the JDOT method [5], which is the starting point of our proposition.

3.1 Optimal Transport

Optimal transport [24] (OT) is a theory that allows to compare probability distributions in a geometrically sound manner. It permits to work on empirical distributions and to exploit the geometry of the data embedding space. Formally, OT searches a probabilistic coupling $\gamma \in \Pi(\mu_1, \mu_2)$ between two distributions μ_1 and μ_2 which yields a minimal displacement cost

$$OT_c(\mu_1, \mu_2) = \inf_{\gamma \in \Pi(\mu_1, \mu_2)} \int_{\mathcal{R}^2} c(\mathbf{x}_1, \mathbf{x}_2) d\gamma(\mathbf{x}_1, \mathbf{x}_2) \quad (1)$$

w.r.t. a given cost function $c(\mathbf{x}_1, \mathbf{x}_2)$ measuring the dissimilarity between samples \mathbf{x}_1 and \mathbf{x}_2 . Here, $\Pi(\mu_1, \mu_2)$ describes the space of joint probability distributions with marginals μ_1 and μ_2 . In a discrete setting (both distributions are empirical) this becomes:

$$OT_c(\mu_1, \mu_2) = \min_{\gamma \in \Pi(\mu_1, \mu_2)} \langle \gamma, \mathbf{C} \rangle_F, \quad (2)$$

where $\langle \cdot, \cdot \rangle_F$ is the Frobenius dot product, $\mathbf{C} \geq 0$ is a cost matrix $\in \mathbb{R}^{n_1 \times n_2}$ representing the pairwise costs $c(\mathbf{x}_i, \mathbf{x}_j)$, and γ is a matrix of size $n_1 \times n_2$ with prescribed marginals. The minimum of this optimization problem can be used as a distance between distributions, and, whenever the cost c is a norm, it is referred to as the Wasserstein distance. Solving equation (2) is a simple linear programming problem with equality constraints, but scales super-quadratically with the size of the sample. Efficient computational schemes were proposed with entropic regularization [30] and/or stochastic versions using the dual formulation of the problem [31, 29, 32], allowing to tackle small to middle sized problems.

3.2 Joint Distribution Optimal Transport

Courty et al. [5] proposed the joint distribution optimal transport (JDOT) method to prevent the two-steps adaptation (i.e. first adapt the representation and then learn the classifier on the adapted features) by directly learning a classifier embedded in the cost function c . The underlying idea is to align the joint features/labels distribution instead of only considering the features distribution. Consequently, μ_s and μ_t are measures of the product space $\mathcal{X} \times \mathcal{Y}$. The generalized cost associated to this space is expressed as a weighted combination of costs in the feature and label spaces, reading

$$d(\mathbf{x}_i^s, \mathbf{y}_i^s; \mathbf{x}_j^t, \mathbf{y}_j^t) = \alpha c(\mathbf{x}_i^s, \mathbf{x}_j^t) + \lambda_t L(\mathbf{y}_i^s, \mathbf{y}_j^t) \quad (3)$$

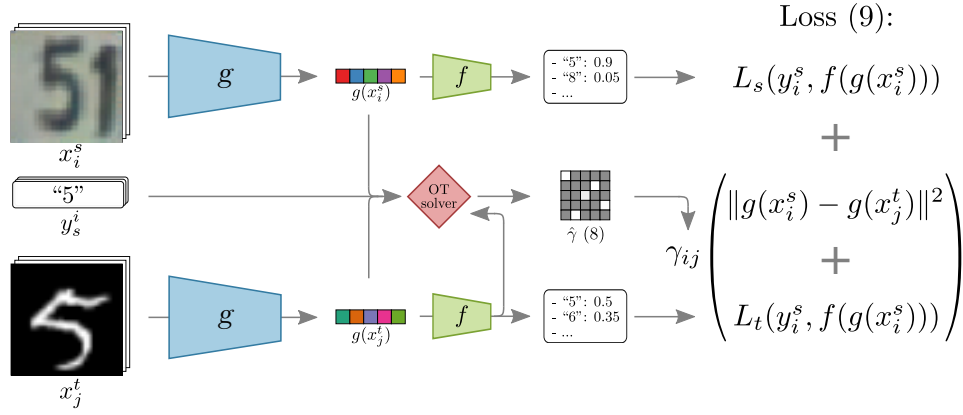


Fig. 1. Overview of the proposed DeepJDOT method. While the structure of the feature extractor g and the classifier f are shared by both domains, they are represented twice to distinguish between the two domains. Both the latent representations and labels are used to compute per batch a coupling matrix γ that is used in the global loss function.

for the i -th source and j -th target element, and where $c(\cdot, \cdot)$ is chosen as a ℓ_2^2 distance and $L(\cdot, \cdot)$ is a classification loss (e.g. hinge or cross-entropy). Parameters α and λ_t are two scalar values weighing the contributions of distance terms. Since target labels \mathbf{y}_j^t are unknown, they are replaced by a surrogate version $f(\mathbf{x}_j^t)$, which depends on a classifier $f : \mathcal{X} \rightarrow \mathcal{Y}$. Accounting for the classification loss leads to the following minimization problem:

$$\min_{f, \gamma \in \Pi(\mu_s, \mu_t)} < \gamma, \mathbf{D}_f >_F, \quad (4)$$

where \mathbf{D}_f depends on f and gathers all the pairwise costs $d(\cdot, \cdot)$. As a by-product of this optimization problem, samples that share a common representation and a common label (through classification) are matched, yielding better discrimination. Interestingly, it is proven in [5] that minimizing this quantity is equivalent to minimizing a learning bound on the domain adaptation problem. However, JDOT has two major drawbacks: *i*) on large datasets, solving for γ becomes intractable because γ scales quadratically in size to the number of samples; *ii*) the cost $c(\mathbf{x}_i^s, \mathbf{x}_j^t)$ is taken in the input space as the squared Euclidean norm on images and can be uninformative of the dissimilarity between two samples. Our proposed DeepJDOT solves those two issues by introducing a stochastic version computing only small couplings along the iterations of a CNN, and by the fact that the optimal transport is learned between the semantic representations in the deeper layers of the CNN, rather than in the image space.

4 Proposed method

4.1 Deep Joint Distribution Optimal Transport(DeepJDOT)

The DeepJDOT model, illustrated in Fig. 1, is composed of two parts: an embedding function $g : \mathbf{x} \rightarrow \mathbf{z}$, where the input is mapped into the latent space

Z , and the classifier $f : \mathbf{z} \rightarrow \mathbf{y}$, which maps the latent space to the label space on the target domain. The latent space can be any feature layer provided by a model, as in our case the penultimate fully connected layer of a CNN. DeepJDOT optimizes jointly this feature space and the classifier to provide a method that performs well on the target domain. The solution to this problem can be achieved by minimizing the following objective function:

$$\min_{\gamma \in \Pi(\mu_s, \mu_t), f, g} \sum_i \sum_j \gamma_{ij} d(g(\mathbf{x}_i^s), \mathbf{y}_i^s; g(\mathbf{x}_j^t), f(g(\mathbf{x}_j^t))), \quad (5)$$

where $d(g(\mathbf{x}_i^s), \mathbf{y}_i^s; g(\mathbf{x}_j^t), f(g(\mathbf{x}_j^t))) = \alpha \|g(\mathbf{x}_i^s) - g(\mathbf{x}_j^t)\|^2 + \lambda_t L(y_i^s, f(g(\mathbf{x}_j^t)))$, and α and λ_t are the parameters controlling the tradeoff between the two terms, as in equation (3). Similarly to JDOT, the first term in the loss compares the compatibility of the embeddings for the source and target domain, while the second term considers the classifier f learned in the target domain and its regularity with respect to the labels available in the source. Despite similarities with the formulation of JDOT [5], our proposition comes with the notable difference that, in DeepJDOT, the Wasserstein distance is minimized between the joint (embedded space/label) distributions within the CNN, rather than between the original input spaces. As the deeper layers of a CNN encode both spatial and semantic information, we believe them to be more apt to describe the image content for both domains, rather than the original features that are affected by a number of factors such as illumination, pose or relative position of objects.

One can note that the formulation reported in equation (5) only depends on the classifier learned in the target domain. By doing so, one puts the emphasis on learning a good classifier for the target domain, and disregards the performance of the classifier when considering source samples. In recent literature, such a degradation in the source domain has been named ‘*catastrophic forgetting*’ [33, 34]. To avoid such forgetting, one can easily re-incorporate the loss on the source domain in (5), leading to the final DeepJDOT objective:

$$\min_{\gamma, f, g} \frac{1}{n^s} \sum_i L_s(y_i^s, f(g(\mathbf{x}_i^s))) + \sum_{i,j} \gamma_{ij} (\alpha \|g(\mathbf{x}_i^s) - g(\mathbf{x}_j^t)\|^2 + \lambda_t L_t(y_i^s, f(g(\mathbf{x}_j^t)))) . \quad (6)$$

This last formulation is the optimization problem solved by DeepJDOT. However, for large sample sizes the constraint of computing a full γ yields a computationally infeasible problem, both in terms of memory and time complexity. In the next section, we propose an approximation method based on stochastic optimization.

4.2 Solving the optimization problem with stochastic gradients

In this section, we describe the approximate optimization procedure for solving DeepJDOT. Equation (6) involves two groups of variables to be optimized: the OT matrix γ and the models f and g . This suggests the use of an alternative

minimization approach (as proposed in the original JDOT). Indeed, when \hat{g} and \hat{f} are fixed, solving equation (6) boils down to a standard OT problem with associated cost matrix $C_{ij} = \alpha \|\hat{g}(x_i^s) - \hat{g}(x_j^t)\|^2 + \lambda_t L_t(y_i^s, \hat{f}(\hat{g}(x_j^t)))$. When fixing \hat{g} , optimizing g and f is a classical deep learning problem. However, computing the optimal coupling with the classical OT solvers is not scalable to large-scale datasets. Despite some recent development for large scale OT with general ground loss [31, 32], the model does not scale sufficiently to meet requirements of recent computer vision tasks.

Therefore, in this work we propose to solve the problem with a stochastic approximation using minibatches from both the source and target domains [35]. This approach has two major advantages: it is scalable to large datasets and can be easily integrated in modern deep learning frameworks. More specifically, the objective function (6) is approximated by sampling a mini-batch of size m , leading to the following optimization problem:

$$\min_{f,g} \mathbb{E} \left[\frac{1}{m} \sum_{i=1}^m L_s(y_i^s, f(g(x_i^s))) + \min_{\gamma \in \Delta} \sum_{i,j} \gamma_{ij} (\alpha \|g(x_i^s) - g(x_j^t)\|^2 + \lambda_t L_t(y_i^s, f(g(x_j^t)))) \right] \quad (7)$$

where \mathbb{E} is the expected value with respect to the randomly sampled minibatches drawn from both source and target domains. The classification loss functions for the source (L_s) and target (L_t) domains can be any general class of loss functions that are twice differentiable. We opted for a traditional cross-entropy loss in both cases. Note that, as discussed in [35], the expected value over the minibatches does not converge to the true OT coupling between every pair of samples, which might then lead to the appearance of connections between samples that would not have been connected in the full coupling. However, this can also be seen as a regularization that will promote sharing of the mass between neighboring samples. Finally note that we did not use the regularized version of OT as in [35], since it introduces an additional regularization parameter that should be cross-validated, which can make the model calibration even more complex. Still, the extension of DeepJDOT to regularized OT is straightforward and could be beneficial for high-dimensional embeddings g .

Consequently, we propose to obtain the stochastic update for Eq.(7) as follows (and summarized in Algorithm 1):

1. With fixed CNN parameters (\hat{g}, \hat{f}) and for every randomly drawn minibatch (of m samples), obtain the coupling

$$\min_{\gamma \in \Pi(\mu_s, \mu_t)} \sum_{i,j=1}^m \gamma_{ij} \left(\alpha \|\hat{g}(x_i^s) - \hat{g}(x_j^t)\|^2 + \lambda_t L_t(y_i^s, \hat{f}(\hat{g}(x_j^t))) \right) \quad (8)$$

using the network simplex flow algorithm.

2. With fixed coupling $\hat{\gamma}$ obtained at the previous step, update the embedding function (g) and classifier (f) with stochastic gradient update for the

Algorithm 1 DeepJDOT stochastic optimization

Require: \mathbf{x}^s : source domain samples, \mathbf{x}^t : target domain samples, \mathbf{y}^s : source domain labels

- 1: **for** each batch of source ($\mathbf{x}_b^s, \mathbf{y}_b^s$) and target samples (\mathbf{x}_b^t) **do**
 - 2: fix \hat{g} and \hat{f} , solve for γ as in equation (8)
 - 3: fix $\hat{\gamma}$, and update for g and f according to equation (9)
 - 4: **end for**
-

following loss on the minibatch:

$$\frac{1}{m} \sum_{i=1}^m L_s(y_i^s, f(g(x_i^s))) + \sum_{i,j=1}^m \hat{\gamma}_{ij} (\alpha \|g(x_i^s) - g(x_j^t)\|^2 + \lambda_t L_t(y_i^s, f(g(x_j^t)))) . \quad (9)$$

The domain alignment term aligns only the source and target samples with similar activation/labels and the sparse matrix $\hat{\gamma}$ will automatically perform label propagation between source and target samples. The classifier f is simultaneously learnt in both source and target domain.

5 Experimental analysis

In this section, we present a series of experiments dealing with cross-domain classification of digits images. First we present the datasets used, then we provide implementation details, before providing and discussing our results.

5.1 Digit classification datasets

We consider four data sources (domains) from the digits classification field: MNIST [36], USPS [37], MNIST-M, and the Street View House Numbers (SVHN) [38] dataset. Each dataset involves a 10-class classification problem (retrieving numbers 0-9):

- *USPS*. The USPS datasets contains 7‘291 training and 2‘007 test grayscale images of handwritten images, each one of size 16×16 pixels.
- *MNIST*. The MNIST dataset contains 60‘000 training and 10‘000 testing grayscale images of size 28×28 .
- *MNIST M*. We generated the MNIST-M images by following the protocol in [8]. MNIST-M is a variation on MNIST, where the (black) background is replaced by random patches extracted from the Berkeley Segmentation Data Set (BSDS500) [39]. The number of training and testing samples are the same as the MNIST dataset discussed above.
- *SVHN*. The SVHN dataset contains house numbers extracted from Google Street View images. We used the *Format2* version of SVHN, where the images are cropped into 32×32 pixels. Multiple digits can appear in a single

image, the objective is to detect the digit in the center of the image. This dataset contains 73'212 training images, and 26'032 testing images of size $32 \times 32 \times 3$. The respective examples of the each dataset is shown in Figure 2.



Fig. 2. Examples from the MNIST, USPS, SVHN and MNIST-M datasets.

The three following experiments were run (the arrow direction corresponds to the sense of the domain adaptation):

- *USPS* \leftrightarrow *MNIST*. The USPS images are zero-padded to reach the same size as MNIST dataset. The adaptation is considered in both directions: USPS \rightarrow MNIST, and MNIST \rightarrow USPS.
- *SVHN* \rightarrow *MNIST*. The single-channel MNIST images are replicated three times to form a gray 3 channels image, and resized to match the resolution of the SVHN images. Here, the adaptation is considered in only one direction: SVHN \rightarrow MNIST. Adapting SVHN images to MNIST is challenging due to the variations in the SVHN images [8]
- *MNIST* \rightarrow *MNIST-M*. MNIST is considered as the source domain and MNIST-M as the target domain. The color MNIST-M images can be easily identified by a human, however it is challenging for the CNN trained on MNIST, which is only grayscale. Again, the gray scale MNIST images are replicated three times to match the color resolution of the MNIST-M images.

5.2 Implementation details

Optimal transport and regularization In our numerical experiments, we report only non-regularized OT for DeepJDOT. As discussed above it avoids the choice of an additional parameter and on quick experiments we observed no significant differences between a regularized OT (where the regularization is validated) and the exact OT in terms of target accuracy. Surprisingly we also observed that for reasonable sizes of OT minibatches (≈ 1024), solving the exact OT with network flow from The POT Toolbox [40] was more efficient than solving the regularized OT for the small validated regularization parameters.

Architecture DeepJDOT is implemented in keras⁴ as a custom loss function. The embedding function g takes the input and embeds into a 128-dimensional

⁴ <https://keras.io/>

vector: $\text{Conv}(32, 3 \times 3) \rightarrow \text{Conv}(32, 3 \times 3) \rightarrow \text{Pool}(2) \rightarrow \text{Conv}(64, 3 \times 3) \rightarrow \text{Conv}(64, 3 \times 3) \rightarrow \text{Pool}(2) \rightarrow \text{Conv}(128, 3 \times 3) \rightarrow \text{Conv}(128, 3 \times 3) \rightarrow \text{Pool}(2) \rightarrow \text{FC}(128)$, where $\text{Conv}(n, k \times k)$ denotes a convolutional layer with n filters of size $k \times k$ and with stride 1, $\text{P}(k)$ denotes a max-pooling layer with window size $k \times k$ and stride 1, and $\text{FC}(k)$ is a fully connected layer with sigmoid activation function and k neurons. The prediction function f is plugged into the fully connected layer and is followed by a softmax to provide the class scores. The same architecture is used in all experiments.

Training parameters The Adam optimizer is used to update our model. We choose the same learning rate ($\tau = 2e^{-4}$) for all our experiments. For the first ten epochs, we train the network only with the source classification loss (L_s), and then we start using the DeepJDOT loss functions. At this point, we also halve the learning rate. After 10k more iterations, the learning rate is again reduced by a factor 0.1 and continued with 5k more iterations. Note that, in most cases, the training converges in less than 10k iterations. While training, we used a mini-batch size of $m_S = m_T = 500$ from the source and target domains. In order to ensure that the classes are well represented at least in the source domain, we draw 50 samples per class for the source minibatch. Increasing the batch size could potentially improve the performance of the network, however we are limited by computing resources available. Tuning the hyperparameters is important for any method to produce the best results, however in unsupervised domain adaptation it is not feasible to cross-validate the hyperparameters, since the labels are not available in the target domain. Therefore, we fixed $\alpha = 0.001$ and $\lambda_t = 0.0001$ throughout our experiments. We compare our proposed DeepJDOT with the following methods:

- non-adversarial discrepancy methods: CORAL [6], MMD[14], DRCN[41], DSN [42], AssocDA[16],
- adversarial discrepancy methods: DANN[8], ADDA[21],
- adversarial image generation methods: CoGAN[9], and UNIT[18], GenToAdapt[19] and I2I Adapt[20].

To ensure fair comparison, we re-implemented the most relevant competitors (CORAL, MMD, DANN, and ADDA). For the other methods, the results are directly reported from the respective articles.

5.3 Results and discussion

Numerical results. Table 1 summarizes the classification accuracies on the target test dataset in the four adaptation scenarios detailed in Section 5.1. The first row (**source only**) shows the accuracies on target test data achieved with classifiers trained on source data without adaptation, and the last row (**target only**) reports accuracies on the target test data achieved with classifiers trained on the target training data. This last method is considered as an upper bound for our proposed method and can be seen as our gold standard. StochJDOT

Table 1. Classification accuracy on the target test datasets. *Source only* and *target only* refer to training on the respective datasets without domain adaptation and evaluating on the target test dataset. The accuracies reported in the first block are our own implementations, while the second block reports performances from the respective articles. **Bold** and *italic* indicates the best and second best results. The last line reports the performance of DeepJDOT on the source domain.

Method	Adaptation:source→target			
	MNIST → USPS	USPS → MNIST	SVHN → MNIST	MNIST → MNIST-M
Source only	94.8	59.6	60.7	60.8
CORAL [6]	89.33	91.5	59.6	66.5
MMD [14]	88.5	73.5	64.8	72.5
AssocDA [16]	-	-	<i>95.7</i>	<i>89.5</i>
DANN [8]	<i>95.7</i>	90.0	70.8	75.4
ADDA [21]	92.4	93.8	76.0 ⁵	78.8
DRCN [41]	91.8	73.6	81.9	-
DSN [42]	91.3	-	82.7	83.2
CoGAN [9]	91.2	89.1	-	-
UNIT [18]	95.9	<i>93.5</i>	90.5	-
GenToAdapt [19]	95.3	90.8	92.4	-
I2I Adapt [20]	92.1	87.2	80.3	-
StochJDOT	93.6	90.5	67.6	66.7
DeepJDOT (ours)	<i>95.7</i>	96.4	96.7	92.4
target only	95.8	98.7	98.7	96.8
DeepJDOT-source	98.5	94.9	75.7	97.8

(stochastic adaptation of JDOT) refers to the accuracy of our proposed method, when the discrepancy between source and target domain is computed with an ℓ_2 distance in the original image space. Lastly, **DeepJDOT-source** indicates the source data accuracy, after adapting to the target domain, and can be considered a measure of catastrophic forgetting.

The experimental results show that **DeepJDOT** achieves accuracies comparable or higher to the current state-of-the-art methods. In the MNIST → USPS experiment, the source only accuracy is high due to the zero-padding trick used to increase the resolution of USPS images: as a result, the accuracy improved from 87.8% (when the interpolation technique is used) to 94.8%. When the methods in the first block of Table 1 are considered, **DeepJDOT** outperforms the competitors by large margins, except **DANN**, with which we score on tie in the one adaptation task. In the more challenging adaptation settings SVHN→MNIST and MNIST→MNIST-M, **CORAL** [6], **MMD** [14] and adversarial discrepancy-based methods **ADDA**⁵ and **DANN** were not able to adapt well to the target domain. In the case of **AssocDA**[16], we directly reported results from the paper for two reasons: first, we used a similar architecture and second, they also reported accuracies with fixed parameter settings. Compared to their method, the performance gap is lower, but still significant. It is noted that this method uses data augmen-

⁵ For **ADDA**[21] in the SVHN→MNIST adaptation task the accuracy is reported from the paper, as we were not able to further improve the source only accuracy

tation in the MNIST→MNIST-M settings, but is outperformed by **DeepJDOT** even without using any data augmentation. Next, we discuss the performance of our method with respect to the state-of-the-art in the second block of Table 1, where the results are reported from the literature. It is interesting to observe that our method showed impressive performance, with about 3-9% (USPS→MNIST) and 4-16% (SVHN→MNIST) accuracy difference compared to the GAN-based methods. In the MNIST→USPS case, our method has comparable result with the state-of-the-art (**UNIT**), despite **DeepJDOT** not using any complex procedure for generating target images to perform the adaptation.

DeepJDOT learns discriminant features while aligning the distributions in the embedding space. This is in contrast with the non-adversarial [6, 14, 41, 42] and adversarial-based methods [8, 21], which aim only at aligning the distributions without considering the semantic specific relations between the domains. The image generation-based adversarial methods [9, 18–20] and **AssocDA**[16] consider the semantic specific relations between domains, but the experimental result showed that modeling this information by means of optimal transport was more effective.

Finally, the results of **StochJDOT** highlight the importance of computing ground metric of optimal transport in the CNN layers, rather than the image space. Even though **StochJDOT** is computed in the image space, it performs better or comparably to **CORAL** and **MMD** methods. It is noted that in **StochJDOT**, the classifier is directly learned only in the target domain. Finally, we show that our proposed **DeepJDOT** performs well on the original source domain too. The only forgetting observed is a decrease of about 10% in classifying the SVHN source domain samples, which might be due to the large variations in source and target domain samples.

***t*-SNE embeddings** We visualize the quality of the embeddings for the source and target domain learnt by **DeepJDOT**, **StochJDOT** and **DANN** using *t*-SNE embedding on the MNIST→MNIST-M adaptation task (Figure 3). As expected, in the source model the samples from the source domain are well clustered and target samples are more scattered. The *t*-SNE embeddings with the **DANN** were not able to align the distributions well, and this observation also holds for **StochJDOT**. It is noted that **StochJDOT** does not align the distributions, but learns the classifier in target domain directly. The poor embeddings of the target samples with **StochJDOT** shows the necessity of computing the ground metric (cost function) of optimal transport in the deep CNN layers. Finally, **DeepJDOT** perfectly aligns the source domain samples and target domain samples to each other, which explains the good numerical performances reported above. The “tentacle”-shaped and near-perfect separation of the classes in the embedding illustrate the fact that **DeepJDOT** finds an embedding that both aligns the source/target distribution, but also maximizes the margin between the classes.

Ablation study Table 2 reports the results obtained in the USPS→MNIST and MNIST→ MNIST-M cases for models using only parts of our proposed

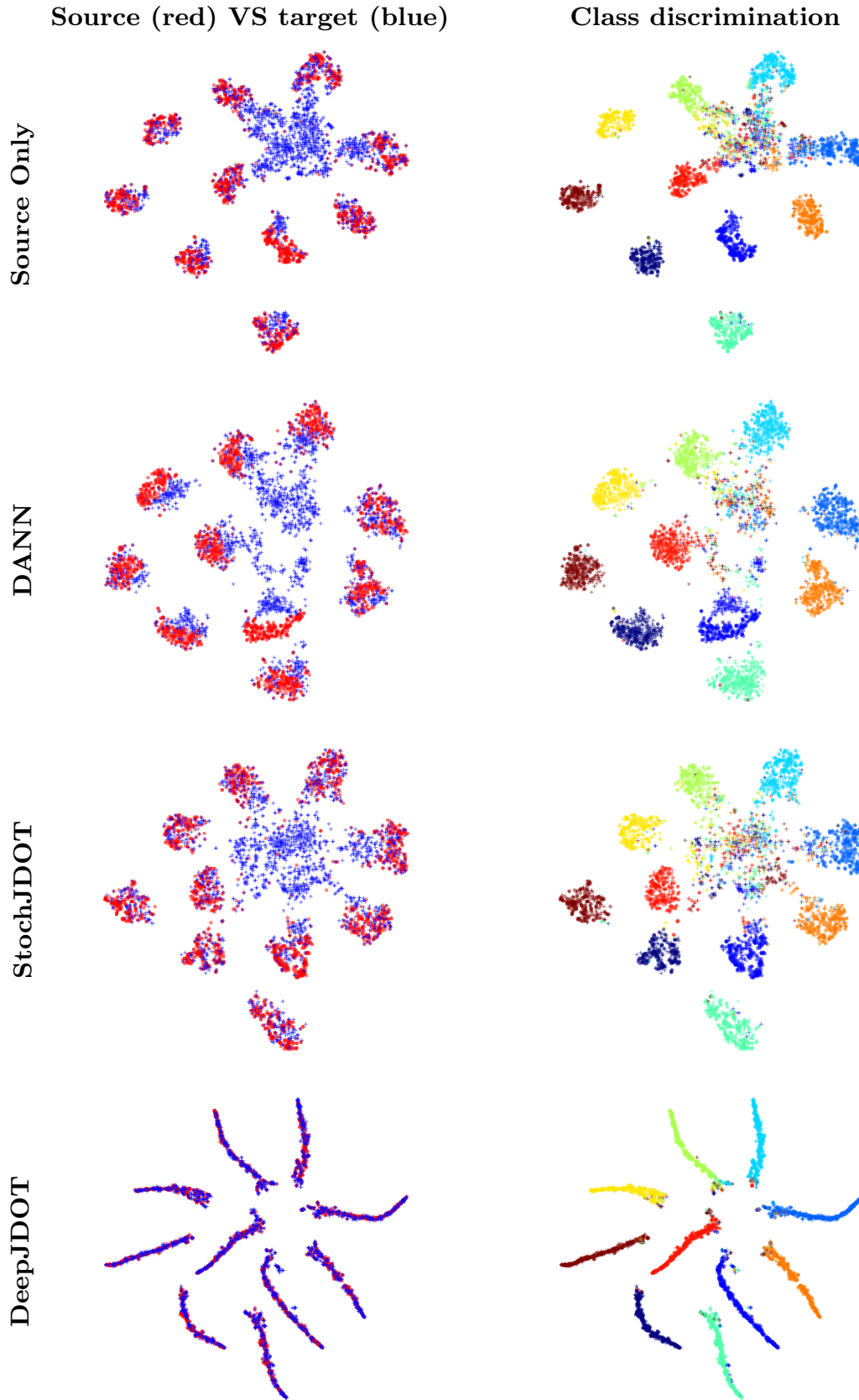


Fig. 3. t-SNE embeddings of 2'000 test samples for MNIST (source) and MNIST-M (target) for **Source only** classifier, **DANN**, **StochJDOT** and **DeepJDOT**. The left column shows domain comparisons, where colors represent the domain. The right column shows the ability of the methods to discriminate classes (samples are colored w.r.t. their classes).

Table 2. Ablation study of DeepJDOT.

Method	USPS \rightarrow MNIST	MNIST \rightarrow MNIST-M
$L_s + (\alpha d + L_t)$	96.4	92.4
$\alpha d + L_t$	86.41	73.6
$L_s + \alpha d$	95.53	82.3

loss (equation (6)). When only the JDOT loss is considered ($\alpha d + L_t$ case), the accuracy drops in both adaptation cases. This behavior might be due to overfitting of the target classifier to the noisy pseudo- (propagated) labels. However, the performance is comparable to non-adversarial discrepancy-based methods reported in Table 1. On the contrary, when only the feature space distribution is included in Equation (6), i.e. the $L_s + \alpha d$ experiment, the accuracy is close to our full model in USPS \rightarrow MNIST direction, but drops in the MNIST \rightarrow MNIST-M one. Overall the accuracies are improved compared to the original JDOT model, which highlights the importance of including the information from the source domain. Moreover, this also highlights the importance of simultaneously updating the classifier both in the source and target domain. Summarizing, this ablation study showed that the individual components bring complimentary information to achieve the best classification results.

6 Conclusions

In this paper, we proposed the DeepJDOT model for unsupervised deep domain adaptation based on optimal transport. The proposed method aims at learning a common latent space for the source and target distributions, that conveys discriminant information for both domains. This is achieved by minimizing the discrepancy of joint deep feature/labels domain distributions by means of optimal transport. We propose an efficient stochastic algorithm that solves this problem, and despite being simple and easily integrable into modern deep learning frameworks, our method outperformed the non-adversarial and adversarial based state-of-the-art on cross domain digits adaptation.

Future works will consider the evaluation of this method in multi-domains scenario, as well as more complicated cost functions taking into account similarities of the representations across the embedding layers and/or similarities of labels across different classifiers.

References

1. Patel, V.M., Gopalan, R., Li, R., Chellappa, R.: Visual domain adaptation: a survey of recent advances. *IEEE SPM* **32**(3) (2015) 53–69
2. Saenko, K., Kulis, B., Fritz, M., Darrell, T.: Adapting visual category models to new domains. In: *ECCV*. (2010) 213–226
3. Gopalan, R., Li, R., Chellappa, R.: Domain adaptation for object recognition: An unsupervised approach. In: *ICCV*. (2011) 999–1006

4. Courty, N., Flamary, R., Tuia, D., Rakotomamonjy, A.: Optimal transport for domain adaptation. *IEEE TPAMI* **39**(9) (2017) 1853–1865
5. Courty, N., Flamary, R., Habrard, A., Rakotomamonjy, A.: Joint distribution optimal transportation for domain adaptation. In: *NIPS*. (2017)
6. Sun, B., Saenko, K.: Deep coral: Correlation alignment for deep domain adaptation. In: *ECCV workshops*. (2016) 443–450
7. Luo, Z., Zou, Y., Hoffman, J., Fei-Fei, L.: Label efficient learning of transferable representations across domains and tasks. In: *NIPS*. (2017)
8. Ganin, Y., Ustinova, E., Ajakan, H., Germain, P., Larochelle, H., Laviolette, F., Marchand, M., Lempitsky, V.: Domain-adversarial training of neural networks. *J. Mach. Learn. Res.* **17**(1) (January 2016) 2096–2030
9. Liu, M.Y., Tuzel, O.: Coupled generative adversarial networks. In Lee, D.D., Sugiyama, M., Luxburg, U.V., Guyon, I., Garnett, R., eds.: *NIPS*. (2016) 469–477
10. Ben-David, S., Blitzer, J., Crammer, K., Pereira, F.: Analysis of representations for domain adaptation. In: *NIPS*. (2007) 137–144
11. Jhuo, I.H., Liu, D., Lee, D.T., Chang, S.F.: Robust visual domain adaptation with low-rank reconstruction. In: *CVPR*. (2012) 2168–2175
12. Hoffman, J., Rodner, E., Donahue, J., Saenko, K., Darrell, T.: Efficient learning of domain-invariant image representations. In: *ICLR*. (2013)
13. Aljundi, R., Tuytelaars, T.: Lightweight unsupervised domain adaptation by convolutional filter reconstruction. In: *ECCV*. (2016)
14. Long, M., Cao, Y., Wang, J., Jordan, M.I.: Learning transferable features with deep adaptation networks. In: *ICML*. (2015) 97–105
15. Long, M., Wang, J., Jordan, M.I.: Unsupervised domain adaptation with residual transfer networks. In: *NIPS*. (2016)
16. Haeusser, P., Frerix, T., Mordvintsev, A., Cremers, D.: Associative domain adaptation. In: *ICCV*. (2017)
17. Tzeng, E., Hoffman, J., Darrell, T., Saenko, K.: Simultaneous deep transfer across domains and tasks. In: *ICCV*. (2015)
18. Liu, M.Y., Breuel, T., Kautz, J.: Unsupervised image-to-image translation networks. In Guyon, I., Luxburg, U.V., Bengio, S., Wallach, H., Fergus, R., Vishwanathan, S., Garnett, R., eds.: *NIPS*. (2017) 700–708
19. Sankaranarayanan, S., Balaji, Y., Castillo, C.D., Chellappa, R.: Generate to adapt: Aligning domains using generative adversarial networks. *CoRR* **abs/1704.01705** (2017)
20. Murez, Z., Kolouri, S., Kriegman, D., Ramamoorthi, R., Kim, K.: Image to Image Translation for Domain Adaptation. *ArXiv e-prints* (December 2017)
21. Tzeng, E., Hoffman, J., Darrell, T., Saenko, K.: Adversarial discriminative domain adaptation. In: *CVPR*. (2017)
22. Monge, G.: *Mémoire sur la théorie des déblais et des remblais*. De l’Imprimerie Royale (1781)
23. Kantorovich, L.: On the translocation of masses. *C.R. (Doklady) Acad. Sci. URSS (N.S.)* **37** (1942) 199–201
24. Villani, C.: *Optimal transport: old and new*. Grundlehren der mathematischen Wissenschaften. Springer (2009)
25. Courty, N., Flamary, R., Tuia, D.: Domain adaptation with regularized optimal transport. In: *ECML*. (2014)
26. Perrot, M., Courty, N., Flamary, R., Habrard, A.: Mapping estimation for discrete optimal transport. In: *NIPS*. (2016) 4197–4205
27. Redko, I., Habrard, A., Sebban, M.: Theoretical analysis of domain adaptation with optimal transport. In: *ECML/PKDD*. (2017) 737–753

28. Shen., J., Qu, Y., Zhang, W., Yu, Y.: Wasserstein distance guided representation learning for domain adaptation. In: AAAI. (2018)
29. Arjovsky, M., Chintala, S., Bottou, L.: Wasserstein generative adversarial networks. In: ICML. (2017) 214–223
30. Cuturi, M.: Sinkhorn distances: Lightspeed computation of optimal transportation. In: NIPS. (2013) 2292–2300
31. Genevay, A., Cuturi, M., Peyré, G., Bach, F.: Stochastic optimization for large-scale optimal transport. In: NIPS. (2016) 3432–3440
32. Seguy, V., Damodaran, B, B., Flamary, R., Courty, N., Rolet, A., Blondel, M.: Large-scale optimal transport and mapping estimation. In: ICLR. (2018)
33. Shmelkov, K., Schmid, C., Alahari, K.: Incremental learning of object detectors without catastrophic forgetting. In: ICCV, Venice, Italy (2017)
34. Li, Z., Hoiem, D.: Learning without forgetting. IEEE TPAMI (in press)
35. Genevay, A., Peyré, G., Cuturi, M.: Sinkhorn-autodiff: Tractable wasserstein learning of generative models. arXiv preprint arXiv:1706.00292 (2017)
36. Lecun, Y., Bottou, L., Bengio, Y., Haffner, P.: Gradient-based learning applied to document recognition. *Proceedings of the IEEE* **86**(11) (Nov 1998) 2278–2324
37. Hull, J.J.: A database for handwritten text recognition research. *IEEE TPAMI* **16**(5) (May 1994) 550–554
38. Netzer, Y., Wang, T., Coates, A., Bissacco, A., Wu, B., Ng, A.Y.: Reading digits in natural images with unsupervised feature learning. In: NIPS worksophs. (2011)
39. Arbelaez, P., Maire, M., Fowlkes, C., Malik, J.: Contour detection and hierarchical image segmentation. *IEEE TPAMI* **33**(5) (May 2011) 898–916
40. Flamary, R., Courty, N.: Pot python optimal transport library. (2017)
41. Ghifary, M., Kleijn, W.B., Zhang, M., Balduzzi, D., Li, W.: Deep reconstruction-classification networks for unsupervised domain adaptation. In: ECCV. (2016) 597–613
42. Bousmalis, K., Trigeorgis, G., Silberman, N., Krishnan, D., Erhan, D.: Domain separation networks. In: NIPS. (2016) 343–351